Low-dose computed tomography image denoising using graph wavelet transform with optimal base

Iwan Setiawan[1,2], Rachmat Hidayat[1], Abdul Mahatir Najar[3], Agus Indra Jaya[3], Didi Rosiyadi[1,2]
[1]Research Center for Artificial Intelligence and Cyber Security, National Research and Innovation Agency (BRIN), Bandung, Indonesia
[2]Center for Research Collaboration on Graph Theory and Combinatorics (BRIN-ITB-UI), Bandung, Indonesia
[3]Department of Physics and Mathematics, Faculty of Mathematics and Natural Science, University of Tadulako, Palu, Indonesia

Article Info

ABSTRACT

Noise in electronic components of computed tomography (CT) detectors behaves like a virus that infects visual quality of CT scans and might distort clinical diagnosis. Modern CT detector technology incorporates high-quality electronic components in conjunction with signal and image processing to ensure optimal image quality while retaining benign doses of x-rays. In this study, a new strategy in signal and image processing directions is proposed by finding the most optimal wavelet base for denoising low-dose CT scan data. The process begins by selecting the appropriate wavelet bases for CT image denoising, followed by a wavelet decomposition, thresholding, and reconstruction. Other methods, such as graph wavelet and learning-based, are used to assess the consistency of the outcomes. The wavelet base of biorthogonal 5.5 achieves the highest optimum performance for CT image denoising. Meanwhile, the Daubechies wavelet base is inconsistent and performs poorly compared to the optimum base. This research highlights the importance of wavelet properties such as orthogonality, regularity, and the number of vanishing moments in selecting an appropriate wavelet basis for noise reduction in CT images.

Corresponding Author:

Iwan Setiawan
Research Center for Artificial Intelligence and Cyber Security, National Research and Innovation Agency
Bandung 40135, Indonesia
Email: iwan022@brin.go.id

1. INTRODUCTION

Noise is always present in medical images, including those acquired by computed tomography (CT). The amount of noise present in the image is determined by the level of radiation dose, with low-dose radiation causing considerable noise in CT images. To minimize the risk of radiation exposure, the dose must be reduced to the lowest possible level while maintaining diagnostic accuracy, particularly for CT exams that may require multiple consecutive scans [1]. Noise on a CT image also depends on the type of CT detector used. Integrated electronic detectors (EIDs) generate less noise than analog detectors due to the presence of an analog-to-digital converter (ADC) [2]. Medical practitioners used iterative reconstruction and filtered back projection techniques to reduce noise or improve the quality of CT images [3]. They also used the projection algorithm to minimize radiation doses [4]. Efforts to reduce CT noise continue even ten years after the discovery of EIDs, with the development of photon-counting detectors (PCDs). This innovative technology offers several advantages, such as a better trade-off between radiation dose and CT image quality than earlier techniques [5]. This enables ultrahigh spatial resolution imaging of scanned objects due to smaller detector pixels and high dose efficiency [6]. However, it is important to preserve the prominent part of the CT scans

with relatively high frequencies to maintain image quality. To achieve this, more advanced techniques like wavelet transform may be necessary.

The development of wavelets began with theoretical work, where the challenge was to formulate the phenomenon and solve physical problems. In the next stage, known as the computational stage, several wavelet applications were developed, one of which is wavelet denoising. This technique involves the use of wavelet decomposition, thresholding, and reconstruction. Wavelet decomposition breaks down the CT images into a set of orthonormal wavelet functions that form a wavelet basis, resulting in four sub-images: approximation, horizontal details, vertical details, and diagonal details. The sub-image approximation contains the low-frequency coefficients for each decomposition level, where the level determines the threshold value. In wavelet thresholding, choosing the optimal wavelet base is significant because it directly affects the wavelet base's ability to approximate the CT images with reduced coefficients. To obtain the reconstructed images, wavelet reconstruction inverts the denoised image back to the original domain. Selection of wavelet bases is a factor that needs consideration. Each wavelet base delivers a different performance for any application. Therefore, selecting the most suitable wavelet base for each specific application, including wavelet denoising, is the main challenge. For example, we must consider how we can be sure that the Haar wavelet used in [7] is the optimal base for CT image denoising.

Selecting an optimal base requires knowledge of wavelet properties such as orthogonality, regularity, and vanishing moment. Orthogonal bases can transform noise from the original domain to the transformed domain while keeping the same statistics [8], protect edges from damage [9], improve peak signal to noise ratio (PSNR) values by reducing mean squared error (MSE) compared to non-orthogonal wavelet bases [10], and provide a sparse representation while keeping the energy intact [11]. Regularity refers to the smoothness of a function and measures the concentration of its energy in the frequency domain. It can identify a sudden shift in data. The regularity of a wavelet has a significant impact on wavelet coefficients in thresholding. It serves a crucial function in wavelet thresholding due to its homogeneity [12]. Although a function's regularity is independent of the number of vanishing moments, the smoothness of some wavelets is related to their vanishing moments, such as biorthogonal wavelets. The number of vanishing moments determines the existence of the function in the wavelet domain. It is the order of the wavelet transform, which is important because the smoothness of the wavelet base is beneficial in reducing the approximation error [13]. However, this does not indicate that being higher is better. Too many vanishing moments may result in the loss of useful information in the signal and the accumulation of useless information, such as noise. The appropriate number of vanishing moments is thus critical to effective wavelet base selection.

This paper presents a discrete wavelet transform for reducing noise in CT images. The objective is to select the optimal base among eligible wavelet bases, construct CT image denoising based on the fluctuation of neighborhood pixels or coefficients, and support the development of CT detectors installed with an image based denoising algorithm involving wavelet transforms and graph theory. This work does not utilize vector based multi-wavelets, which means some desirable wavelet properties cannot be used simultaneously [14]. The challenge of this research is to investigate the effect of coefficient distribution on the performance of wavelet denoising on CT images. Another challenge is to determine the optimal balance between denoising and edge preservation. There is an alternative solution to these issues, which involves the use of graph wavelet-based denoising [15]. This paper is presented in four sections. Section 2 outlines the selection process for the optimal wavelet base for denoising CT images using the proposed algorithm. In Section 3, the discussion moves to experimental findings and compares them with graph wavelet transform and learning-based methods. Lastly, Section 4 presents the conclusion.

2. METHOD

This section provides the optimal strategy for denoising CT images, including finding the optimal wavelet base. The algorithm takes low-dose CT images as input for the initial selection of wavelet bases. First, we collect all wavelet bases available in the literature and then determine which ones pass the initial selection criteria based on wavelet decomposition and thresholding. We consider wavelet properties for image denoising and proceed to the final stage, where we exploit wavelet denoising and reconstruction to obtain the optimal base. The following subsections provide detailed explanations of the method.

2.1. Collecting the data

CT measurements are required to gather data using the setup illustrated in Figure 1. The process starts with scanning the human body using rotary x-rays, followed by signal capture through a detector, which compiles multiple-slice images. These images, acquired with low doses of x-rays, undergo image processing to enhance their quality. To evaluate the proposed method, 30 slices of CT images from [16] will

be used. The selected slices are labeled sequentially, as shown in Figure 2. However, these low-dose CT images contain various types of noise.

The introduction of noise begins with the activation of the CT instrument. One type of noise is random noise, which arises when a limited number of x-rays are projected. This noise leads to fluctuations in the signal, resulting in unpredictable density variations. Another type is electronic noise, generated by interference from electronic components, electrical power supplies, and any devices connected to the power supply network. As the signal captured by the X-ray detector is converted to a digital signal for CT image generation, numerical computations can introduce rounding noise. After this extensive process, the resulting CT images will contain noticeable noise.

The noises on low-dose CT images are typically unknown, which makes quantitatively assessing their quality complicated. Therefore, the rational approach is to use full-dose CT images as reference images to objectively evaluate the performance of the proposed method by calculating their PSNR and structural similarity index (SSIM) values, which (1) and (2) for each labeled image where the values are available in Figure 3 for all labeled images with PSNR in Figure 3(a) and SSIM in Figure 3(b). Because the variability of image quality of the 30 labeled low-dose CT images is very high, the doctor can make inaccurate diagnoses when facing the low quality. Thus, performing a denoising technique on low-dose CT images is necessary.
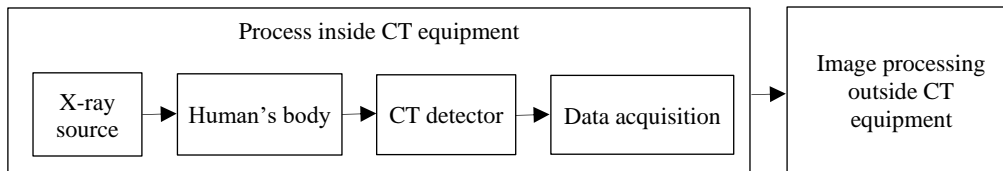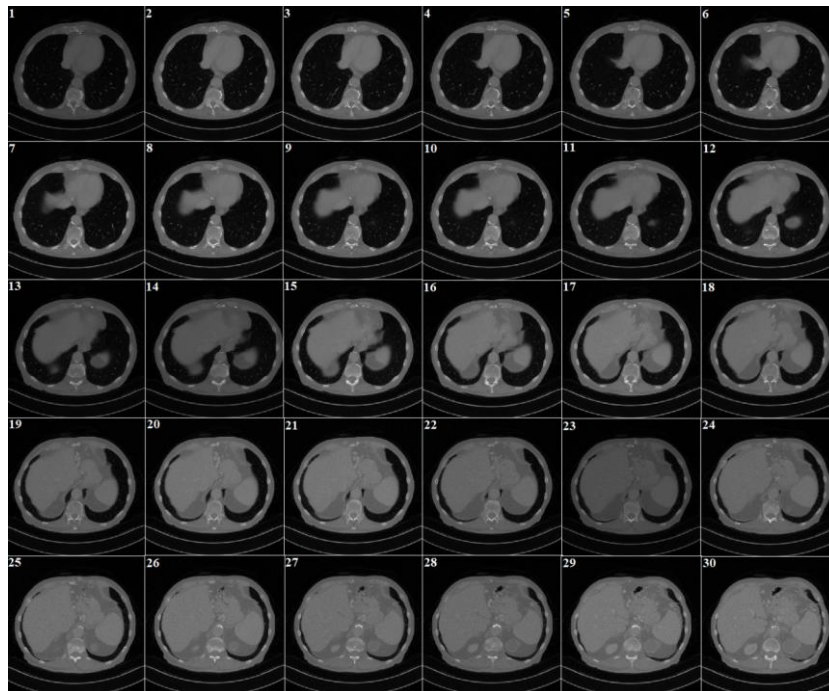

Figure 1. CT scan with image processing

Figure 2. The 30 images from [16]

$$PSNR = 20 \, log_{10} \left(\frac{Max_I}{\sqrt{MSE}} \right) \tag{1}$$

$$SSIM = \frac{(2\mu_x\mu_y + c_1)(2\sigma_{xy} + c_2)}{(\mu_x^2 + \mu_y^2 + c_1)(\sigma_x^2 + \sigma_y^2 + c_2)} \tag{2}$$

where *x, y, μ, σ, σ²*, *c, Max$_i$,* and *MSE* correspond to the low and full-dose pixel, the pixel average, the pixel standard deviation, the pixel variance, parameter corresponds to the dynamic range of the pixel, the maximum possible pixel value of the image, and the mean square error between the low and full-dose, respectively.
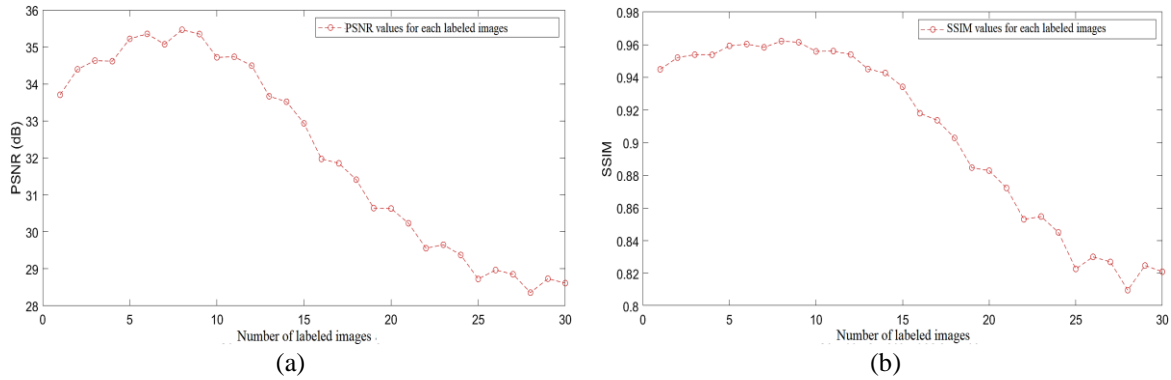

Figure 3. Image quality of the 30 low-dose CT images based on (a) PSNR and (b) SSIM

2.2. Selecting the optimal base

Wavelets possess unique properties that significantly influence their behavior and performance in the denoising of CT images. These properties are essential and serve as the primary criteria for selection. When choosing wavelet bases, it is important to consider their characteristics and how they relate to the specific application. However, it is often unclear why certain bases are used for particular applications. Many users apply wavelets without fully understanding or questioning their properties.

For effective image denoising, the necessary properties include orthogonality, regularity, and vanishing moments. Failing to meet these criteria can lead to suboptimal performance. Table 1 outlines the properties of each wavelet base. All the bases listed in Table 1 satisfy the orthogonality requirement, with the exception of biorthogonal wavelets. Additionally, the Symlet and Coiflet wavelets do not meet the regularity requirement. The Haar, Daubechies, Biorthogonal, and Meyer wavelets meet the additional requirements for regularity and the number of vanishing moments. However, Meyer wavelets fail to fulfill the compact support requirement due to their infinite nature [17]. Thus, to reduce noise in CT images with low-dose x-rays, we will utilize the three wavelet families: Haar, Daubechies, and Biorthogonal.

Table 1. Wavelet bases and their properties

Variable	Requirements for discrete wavelet transformation (DWT) properties		
	Orthogonality	Regularity	Vanishing moments
Haar	☑	☑	☑
Daubechies (Db)	☑	☑	☑
Symlet (Sym)	☑	☒	☑
Coiflet (Coif)	☑	☒	☑
Biorthogonal (Bior)	☒	☑	☑
Meyer (Meyr)	☑	☑	☑

Once the bases are selected, the next step is determining the decomposition level used to transform the noisy images to calculate a wavelet coefficient representing a measure of similarity in the frequency content between the low-dose CT images and the selected wavelet base by performing discrete wavelet transformation (DWT) on the noisy image. The DWT, as shown in Figure 4, provides a multilevel decomposition of an image into approximations and detail coefficients at each level by applying low-pass and high-pass filtering to the rows and columns of the matrix representation of the image [18]. The output of this process produces four images: approximation, horizontal details, vertical details, and diagonal details, as shown in Figure 4(a). In this context, decomposition will be performed only on the low-frequency or approximation coefficients. Otherwise, the study will move to a wavelet packet, which is out of the context of this research. Changing the level of DWT will change the wavelet coefficient, which measures the similarity in the frequency content between the low-dose CT images and the selected wavelet base. As the number of decomposition levels increases, the quality of the decomposition image decreases. It can be proven by

Figure 4(b), which shows the outcome for all low coefficients up to four decomposition levels. The selected level in Figure 4(b) will be processed using wavelet denoising through thresholding, which involves selecting a wavelet base, followed by an inverse transformation to obtain the reconstructed image. Thus, the first level of decomposition is selected, and the coefficient at this level is collected.
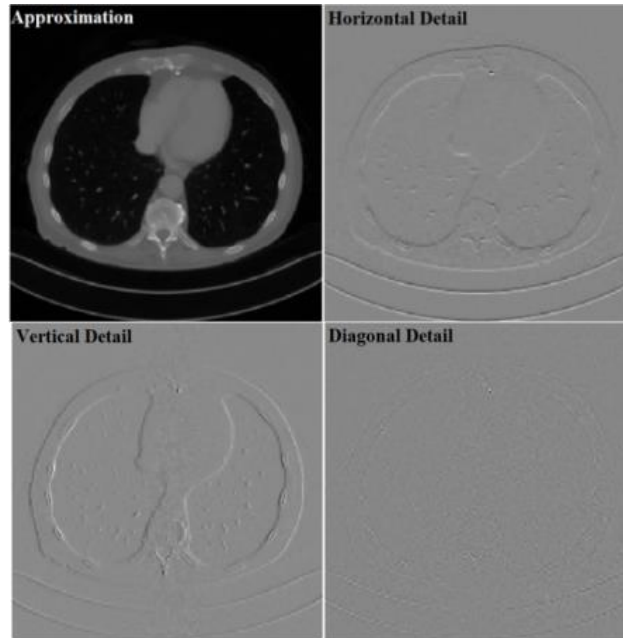
(a)
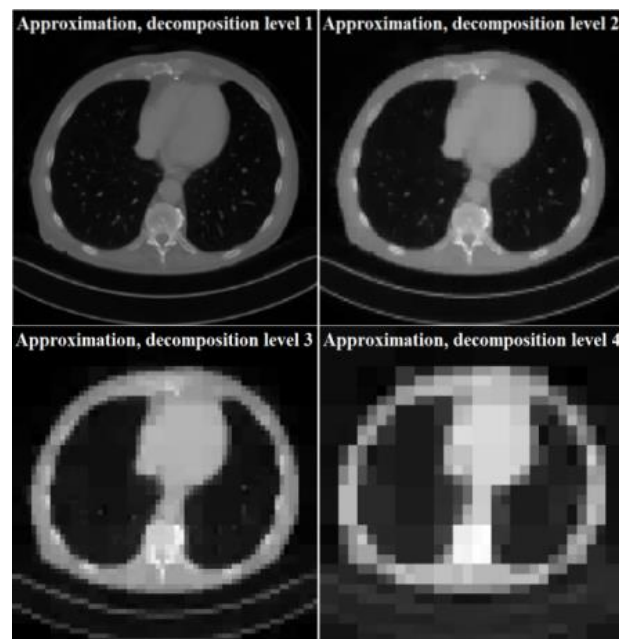
(b)

Figure 4. Wavelet decomposition in (a) level 1 with approximation, horizontal, vertical, and diagonal coefficients and (b) its effect on the approximation coefficients up to level 4

After decomposing the noisy images at a selected level, a wavelet thresholding technique is employed to reduce noise. In this process, values above the threshold are classified as signals, while those below are considered noise. Choosing the appropriate wavelet base is crucial at this stage. By selecting a suitable base, only a limited number of non-zero coefficients are used for noise removal. This approach

results in a higher PSNR and fewer threshold values compared to the RigrSURE, Universal, and MiniMaxi thresholding methods, as demonstrated in Table 2. The results also depend on the images used. However, across both factors, wavelet thresholding yielded the highest PSNR and the lowest threshold values.

Table 2. Comparison of PSNR (in dB) and threshold values between wavelet and other thresholding methods for the chosen slice, Haar wavelet, and the base representing Daubechies and biorthogonal wavelets

Variable	Thresholding techniques							
	RigrSURE		Universal		MiniMaxi		Wavelet	
	Threshold	PSNR	Threshold	PSNR	Threshold	PSNR	Threshold	PSNR
Haar	0.0315	26.913	3.3302	26.908	1.8568	26.908	0.0032	30.573
Daubechies (Db6)	0.0310	28.856	3.3314	28.856	1.8578	28.856	0.0032	32.761
Biorthogonal (Bior5.5)	0.0338	29.750	3.3394	29.750	1.8649	29.750	0.0034	33.997

In the next section, we will show that these values affect the denoising performance based on the PSNR values of the reconstructed CT images. We used various tools such as the spectral graph wavelet transform (SGWT) [19], low-dose computed tomography (LDCT) [20], residual encoder-decoder convolutional neural network (RED-CNN) [21], conveying path-based convolutional encoder-decoder (CPCE) [22], Wasserstein general adversarial network (WGAN) [23], nonlocal network (NLnet) [24], and adaptive global context-based long-short residual encoder-decoder (AGC-LSRED) [25] to evaluate the performance of the results. We can find the code link and algorithm for SGWT at [19]. The PSNR values for the reconstructed CT images of patient L506 using LDCT, RED-CNN, CPCE, WGAN, NLnet, and AGC-LSRED can be found at [25].

2.3. Denoising the images

After collecting the images and selecting the optimal wavelet base, the next step involves processing the images on a personal computer to reduce the noise using image processing techniques by performing the optimal base to obtain a denoised image with the best performance. Before applying a suitable denoising technique, understanding the noise distribution is required. Although the noise distribution in the CT image is often unknown, the Poisson and Gaussian distributions are good options. In other medical images, such as conventional X-ray scans and magnetic resonance images, various types of noise, including speckle noise and salt-and-pepper noise, are present in addition to the former noise. On this step, the noisy image will be processed, the reconstructed image will be assessed, and the performance will be compared and validated.

Preprocessing the pixel values before transforming the image allows for better noise capture. One way to achieve this is by converting the image matrix into a graph matrix. The combination of the graph approach with the wavelet transform is known as the graph wavelet transform. This process follows a specific algorithm that consists of two working domains, which are the spatial and frequency domains. In the spatial domain, the first thing to do is calculate the adjacency matrix values for each pixel by identifying its neighbors as shown in Figure 5. For a 512×512 image in Figure 5(a), the matrix will be of size 262144×262144, with 1046528 elements having a value of one and 6.8718×10^{10} elements having a value of zero, creating a sparse matrix as shown in Figure 5(b).

The second step in the spatial domain is to determine the Laplacian matrix by calculating each element using (3). The variables v, r, c, i, and L represent the vertex, row, column, number of vertices, and Laplacian matrix, respectively. Refer to Figure 6 for a visual representation. The elements of the Laplacian matrix are defined as follows: (a) In Figure 6(a), the element for the first vertex (v_1) is equal to 2 because it has two edges, located in the first row (r_1) and the first column (c_1). (b) In Figure 6(b), the element for the second vertex (v_2) is equal to 3 due to its three edges, found in the first row (r_1) and the second column (c_2). (c) In Figure 6(c), the element for the 514th vertex (v_{514}) is equal to 4 because it has four edges, located in the second row (r_2) and the second column (c_2). The whole element matrix creates a Laplacian matrix with size 262144×262144, where 1308672 nondiagonal elements and 262144 diagonals have values, and the remaining elements are zeros, as illustrated in Figure 7.
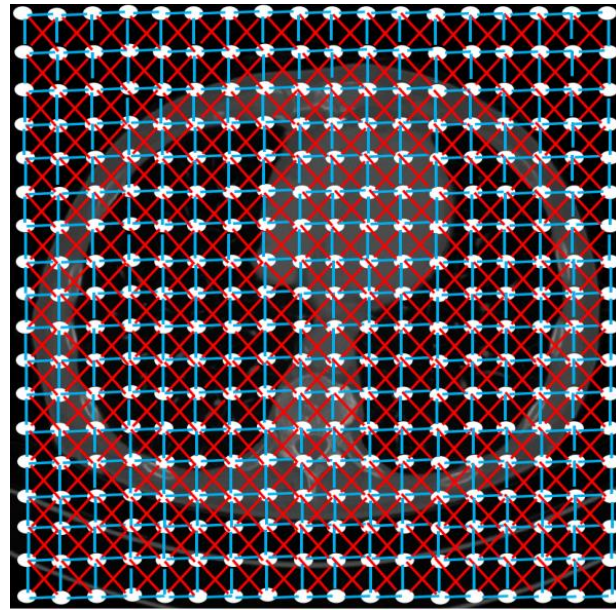
$$L(r,c) = \begin{cases} d(v_i); & \text{if } r = c \\ -1; & \text{if } r \neq c \text{ and } v_r \text{ is adjacent to } v_c \\ 0; & \text{otherwise} \end{cases} \tag{3}$$

The eigenvalue serves as a link between the spatial and frequency domains. It is calculated using (4), where L represents the Laplacian matrix depicted in Figure 7, x denotes the eigenvector, and λ symbolizes the eigenvalue. Unfortunately, an analytical solution to this equation is not feasible due to the large size of the matrix L, which is 262144×262144. This size can disrupt the sparsity structure of the

Laplacian matrix. Consequently, the eigenvalues, which are the solutions to this equation, are determined using an iterative method.

$$L \begin{bmatrix} v_1 \\ \vdots \\ v_n \end{bmatrix} = \begin{bmatrix} \lambda_1 & \cdots & 0 \\ \vdots & \ddots & \vdots \\ 0 & \cdots & \lambda_n \end{bmatrix} \begin{bmatrix} v_1 \\ \vdots \\ v_n \end{bmatrix} \tag{4}$$

These eigenvalues are used to determine the wavelet filter as a function of scale. This wavelet filter with a scaling function is required to calculate the Chebyshev coefficient. Use this Chebyshev coefficient representing the wavelet and the Laplacian matrix representing the graph to transform the low-dose CT images by calculating the transform coefficient. Finally, by performing an inverse graph wavelet transform, the reconstructed images of the low-dose CT will be obtained. Detailed work on this step is available in [26].

(a)

(b)

Figure 5. The adjacency matrix corresponds to (a) 512×512 pixel and (b) 262144×262144 matrix elements
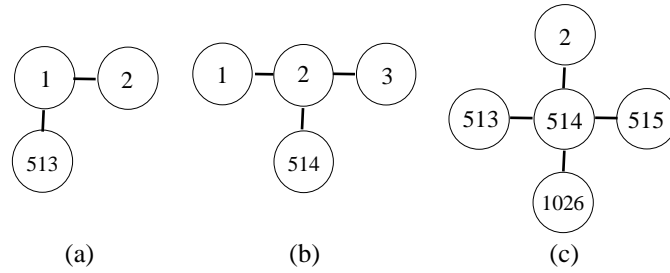
Figure 6. The way to determine Laplacian matrix correspond to the (a) first, (b) second, and (c) 514th vertex

Figure 7. Laplacian matrix with size 262144×262144

3. RESULTS AND DISCUSSION

3.1. Thresholding evaluation

Thresholding is a technique used to eliminate certain coefficients from a noisy image. Coefficients that fall below a specified threshold value are removed, as they are assumed to represent noise. While different methods exist for determining the threshold value, they all operate under the assumption that noise follows a Gaussian distribution, which requires noise level estimation. When using DWT, the noise level is estimated by calculating the median of the absolute values of the wavelet coefficients. This estimation yields a threshold value (T) for wavelet denoising, which is derived from the calculations represented in (5). It is important to adapt this threshold for various methods, including stein's unbiased estimate of risk (SURE), universal, and MiniMaxi thresholding.

$$T = \frac{median\left(abs(c_{approximation})\right)}{0.6745}\sqrt{2\log n} \tag{5}$$

Wavelet thresholding is a method used to reduce noise in images. This process involves removing wavelet coefficients that fall below a predetermined threshold. These coefficients are obtained through wavelet decomposition, where larger coefficients indicate important image content and smaller coefficients typically represent noise. The threshold value is determined based on the characteristics of these coefficients. By adjusting the relevant coefficients appropriately using wavelet thresholding, we can effectively reduce noise in the data. The coefficients derived from the noisy image provide a clearer representation. However, when a single global threshold is applied, wavelet thresholding can estimate noise levels in a specific orientation. The accuracy of this estimation may decline at higher noise levels due to diagonal edges present in the approximation coefficients. To preserve local regularity in the image, it is essential to consider the vanishing moments and regularity properties of the wavelet basis when thresholding these coefficients.

Using biorthogonal wavelets leads to better results when the wavelets have higher vanishing moments. This is particularly effective because the presence of sparsely spaced transients in a noisy image allows for more efficient representation. Biorthogonal wavelets, which consist of two scaling functions and two wavelet functions, offer improved regularity compared to orthogonal wavelets, such as the Daubechies wavelet. This enhanced regularity results in a smoother reconstructed image. Additionally, biorthogonal wavelet filters are symmetric and exhibit linear phase characteristics, which are essential for image processing. This symmetry helps prevent the introduction of visual distortions in the image. The use of a biorthogonal wavelet with many vanishing moments results in fewer significant wavelet coefficients, allowing for more coefficients to be reduced during the denoising process. However, it's important to note that using an analysis filter with fewer vanishing moments than a synthesis filter can adversely affect the denoising results. Furthermore, the DWT with a biorthogonal wavelet does not conserve energy, as energy is not preserved during the analysis stage.

A comparison of threshold values using wavelet thresholding is presented in Figure 8, where the values for wavelet across all suitable bases outperform the Universal and MiniMaxi in Figure 8(a) and SURE in Figure 8(b), which means it will reduce wavelet coefficients less than other methods. This implies that using wavelet thresholding for denoising medical images is beneficial. After applying thresholding to remove noise from the wavelet coefficients, all the coefficients are reduced to form a denoised image. The next step is to reconstruct the denoised image by transforming it back to its original form using the inverse DWT.
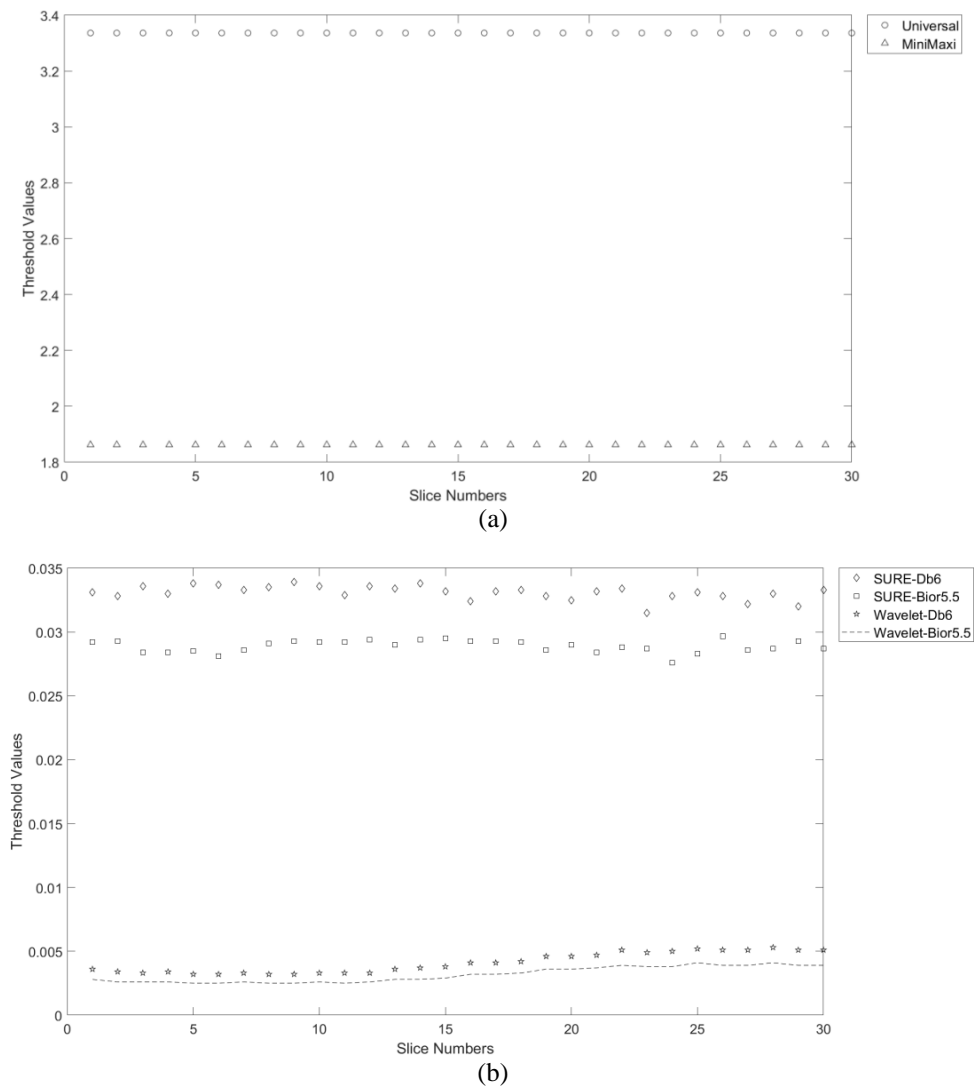

(a)

(b)

Figure 8. Threshold value for (a) universal and MiniMaxi (b) SURE and wavelet

3.2. Graph-based amelioration

A graph wavelet transform is necessary because the sparse representation produced by wavelet decomposition cannot be sufficiently addressed by wavelet thresholding alone. This can be demonstrated by comparing the results of wavelet thresholding with those obtained from the graph-based wavelet transform, as illustrated in Table 3. This table also evaluates the best performance of denoised image reconstruction across various methods, including learning-based approaches applied to all slice numbers. The results indicate that the graph wavelet transform outperforms all other methods for CT images across all L506 slices.

The Objective values obtained after reconstructing the denoised images using all the methods are presented in Figure 9, for 30 numbers of CT slice images. Based on the PSNR and SSIM presented in Figures 9(a) and 9(b), respectively, we conclude that the most suitable base for wavelet denoising application to low-dose CT images is Biorthogonal 5.5. For visual assessment, Figure 10 shows a comparison between Bior5.5 and Db6 with scan 8 and its region of interest in Figure 10(a), where Bior5.5 achieves better than Db6 by comparing Figure 10(b) with Figure 10(c). Db6 was chosen to represent the Daubechies wavelet family since it has the best PSNR values within the family. Scan 8 was chosen because it produces the highest PSNR values for both wavelet thresholding and graph wavelet transform. Figure 11 shows that Bior5.5 graph wavelet transform is better than Bior5.5 wavelet thresholding in denoising the low-dose image with respect to the full dose in Figures 11(a) by comparing Figure 11(b) with Figure 11(c).

Table 3. Comparison of the best PSNR (in dB) for all the methods and L506 slices reconstructed CT images

Measured performance	Methods							
	LDCT	RED-CNN	CPCE	WGAN	NLnet	AGC-LSRED	Wavelet	Graph wavelet
PSNR	27.24 [25]	32.93 [25]	33.04 [25]	30.80 [25]	33.06 [25]	33.17 [25]	34.06	35.47
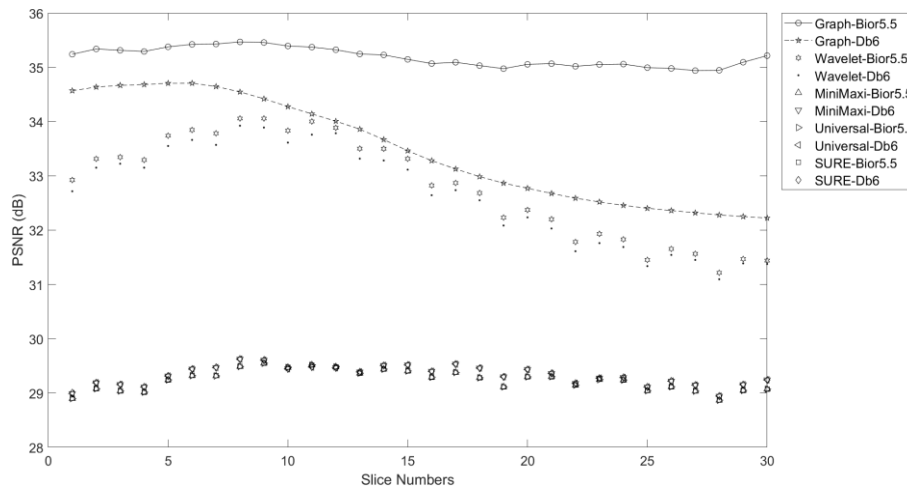
(a)
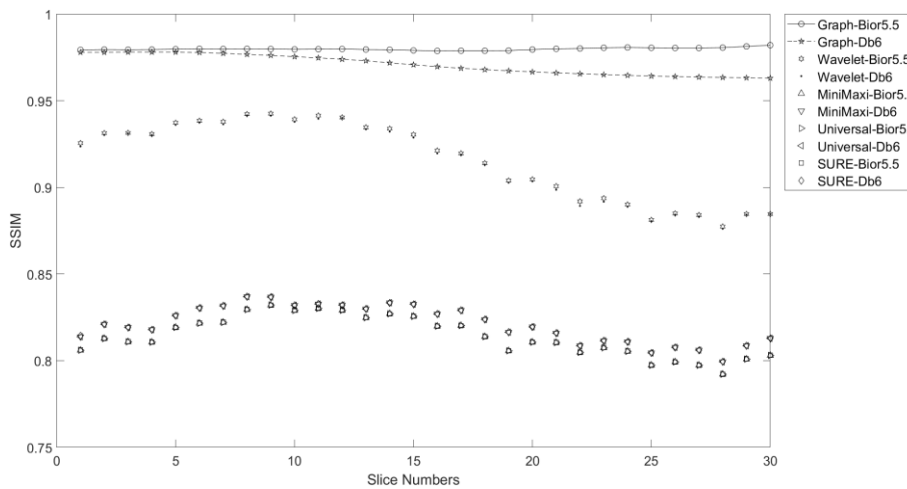
(b)

Figure 9. Comparison of (a) PSNR and (b) SSIM for all methods and the 30 reconstructed images
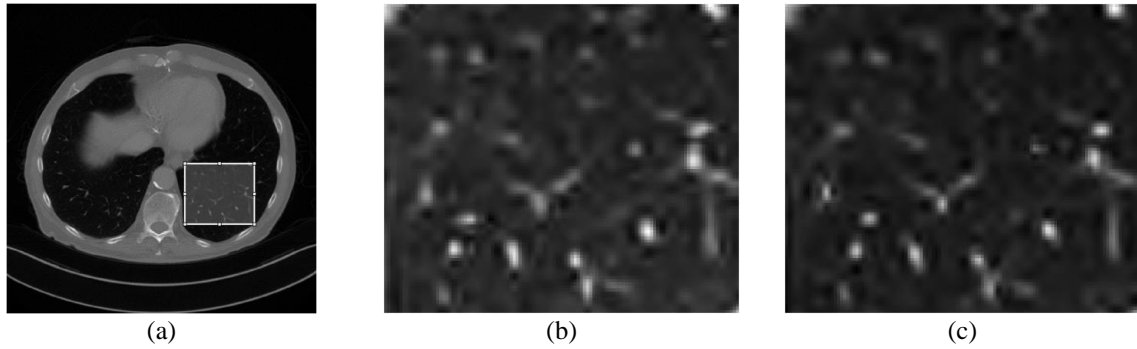
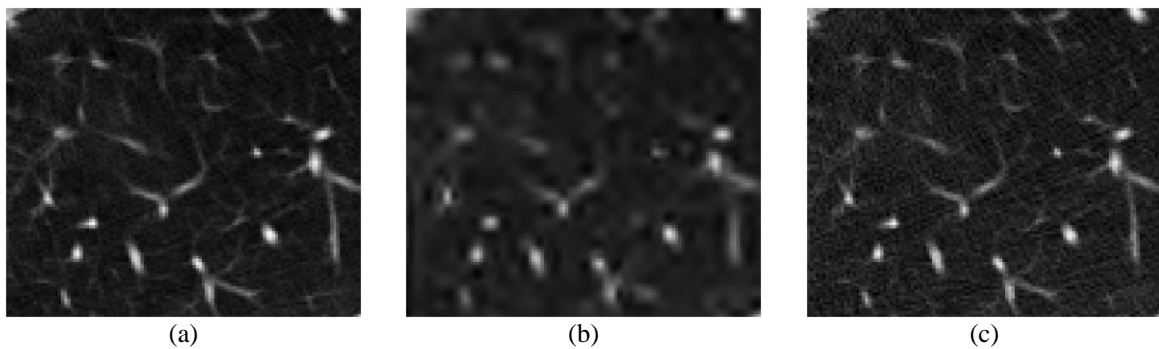Figure 10. L506 CT image with scan labeled 8 in (a) region of interest (RoI) (b) Db6 and (c) Bior5.5

Figure 11. L506 CT image with scan labeled 8 in (a) full dose (b) Bior5.5 wavelet (c) Bior5.5 graph wavelet

3.2. Statistical validation

A Wilcoxon rank-sum test was performed to validate the results of this paper. This test assumed that the 30 data points, which represent reconstructed images obtained from image denoising using the Db6 and Bior5.5 wavelet transform, are independent. P-values were calculated to compare the 30 data samples with the null hypothesis of equal medians against the alternative hypothesis of unequal medians. Table 4 demonstrates that only the graph wavelet transform satisfies the hypothesis for both the peak signal-to-noise ratio (PSNR) and SSIM. A result of h=1 indicates rejection of the null hypothesis, while h=0 indicates a failure to reject it at the 5% significance level. However, wavelet thresholding did not meet the statistical criteria across all quality measures for both parameters. In contrast, methods utilizing SURE, Universal, and MiniMaxi thresholding support the hypothesis only when assessing SSIM. Overall, these findings suggest that the graph wavelet transform is the optimal choice for denoising low-dose CT images.

Table 4. Statistically validating the results for Db6 and Bior5.5

Measured performance	Model to be statistically validated: Db6 and Bior5.5					Wilcoxon rank-sum test
	RigrSURE	Universal	MiniMaxi	Wavelet	Graph wavelet	
PSNR	0	0	0	0	1	h
	$9.05 \times 10{-}2$	$9.19 \times 10{-}2$	$9.19 \times 10{-}2$	$4.04 \times 10{-}1$	$3.02 \times 10{-}11$	p
SSIM	1	1	1	0	1	h
	$1.80 \times 10{-}2$	$1.76 \times 10{-}2$	$1.76 \times 10{-}2$	$6.36 \times 10{-}1$	$2.97 \times 10{-}11$	p

4. CONCLUSION

The experiment demonstrates that selecting the appropriate wavelet basis is essential for denoising low-dose CT images, yielding the best results as measured by PSNR and SSIM. We evaluated various methods, including the thresholding technique, to determine the most effective wavelet basis. Our analysis includes comparing wavelet thresholding techniques, graph wavelets, and learning-based methods for reconstructing denoised CT images. Based on the PSNR and SSIM performance metrics, the graph-based wavelet denoising technique provides superior image quality, effectively addressing the noise issues in low-dose CT images when compared to RigrSURE, Universal, MiniMaxi, and conventional wavelet thresholding

methods. Future research could explore the potential of applying learning-based techniques to graph wavelets, rather than limiting the approach to either wavelet or graph methods alone.

REFERENCES

[1] S. Poosiri, A. Krisanachinda, and K. Khamwan, "Evaluation of patient radiation dose and risk of cancer from CT examinations," *Radiological Physics and Technology*, vol. 17, no. 1, pp. 176–185, Mar. 2024, doi: 10.1007/s12194-023-00763-w.

[2] M. Lell and M. Kachelrieß, "Computed tomography 2.0: new detector technology, AI, and other developments," *Investigative Radiology*, vol. 58, no. 8, pp. 587–601, Jun. 2023, doi: 10.1097/RLI.0000000000000995.

[3] Q. Bellmann, Y. Peng, U. Genske, L. Yan, M. Wagner, and P. Jahnke, "Low-contrast lesion detection in neck CT: a multireader study comparing deep learning, iterative, and filtered back projection reconstructions using realistic phantoms," *European Radiology Experimental*, vol. 8, no. 1, p. 84, Jul. 2024, doi: 10.1186/s41747-024-00486-6.

[4] M. Takemitsu, S. Kudomi, K. Takegami, and T. Uehara, "The effect of a pre-reconstruction process in a filtered back projection reconstruction on an image quality of a low tube voltage computed tomography," *Radiological Physics and Technology*, vol. 17, no. 1, pp. 306–314, Mar. 2024, doi: 10.1007/s12194-023-00764-9.

[5] A. A. Marth, R. P. Marcus, G. C. Feuerriegel, D. Nanz, and R. Sutter, "Photon-counting detector CT versus energy-integrating detector CT of the lumbar spine: comparison of radiation dose and image quality," *American Journal of Roentgenology*, vol. 222, no. 1, Jan. 2024, doi: 10.2214/AJR.23.29950.

[6] F. I. Baffour *et al.*, "Photon-counting detector CT for musculoskeletal imaging: a clinical perspective," *American Journal of Roentgenology*, vol. 220, no. 4, pp. 551–560, Apr. 2023, doi: 10.2214/AJR.22.28418.

[7] T. K. Abuya, R. M. Rimiru, and G. O. Okeyo, "An image denoising technique using wavelet-anisotropic gaussian filter-based denoising convolutional neural network for CT images," *Applied Sciences*, vol. 13, no. 21, p. 12069, Nov. 2023, doi: 10.3390/app132112069.

[8] A. Guillet and F. Argoul, "Uncertainty and information in physiological signals: explicit physical trade-off with log-normal wavelets," *Journal of the Franklin Institute*, vol. 361, no. 18, p. 107201, Dec. 2024, doi: 10.1016/j.jfranklin.2024.107201.

[9] X. Xue, D. Ji, C. Xu, Y. Zhao, Y. Li, and C. Hu, "Adaptive orthogonal directional total variation with kernel regression for CT image denoising," *Journal of X-Ray Science and Technology*, vol. 32, no. 5, pp. 1253–1271, Sep. 2024, doi: 10.3233/XST-230416.

[10] G. Wang, S. Guo, L. Han, A. B. Cekderi, X. Song, and Z. Zhao, "Asymptomatic COVID-19 CT image denoising method based on wavelet transform combined with improved PSO," *Biomedical Signal Processing and Control*, vol. 76, p. 103707, Jul. 2022, doi: 10.1016/j.bspc.2022.103707.

[11] X. Li, W. Wan, F. Zhou, X. Cheng, Y. Jie, and H. Tan, "Medical image fusion based on sparse representation and neighbor energy activity," *Biomedical Signal Processing and Control*, vol. 80, p. 104353, Feb. 2023, doi: 10.1016/j.bspc.2022.104353.

[12] A. V Perez-Sanchez, J. P. Amezquita-Sanchez, M. Valtierra-Rodriguez, and H. Adeli, "A new epileptic seizure prediction model based on maximal overlap discrete wavelet packet transform, homogeneity index, and machine learning using ECG signals," *Biomedical Signal Processing and Control*, vol. 88, p. 105659, Feb. 2024, doi: 10.1016/j.bspc.2023.105659.

[13] K.-H. Seo, S.-H. Kang, J. Shim, and Y. Lee, "Optimization of smoothing factor for fast non-local means algorithm in high pitch based low-dose computed tomography images with tin-filter," *Radiation Physics and Chemistry*, vol. 206, p. 110762, May 2023, doi: 10.1016/j.radphyschem.2023.110762.

[14] M. Majeed Laftah, "Image denoising using multiwavelet transform with different filters and rules," *International Journal of Interactive Mobile Technologies (iJIM)*, vol. 15, no. 15, p. 140, Aug. 2021, doi: 10.3991/ijim.v15i15.24183.

[15] B. de Loynes, F. Navarro, and B. Olivier, "data-driven thresholding in denoising with spectral graph wavelet transform," *Journal of Computational and Applied Mathematics*, vol. 389, 2021, doi: 10.1016/j.cam.2020.113319.

[16] L. Armato III, SG; McLennan, G; Bidaut, L; McNitt-Gray, MF; Meyer, CR; Reeves, AP; Zhao, B; Aberle, DR; Henschke, CI; Hoffman, Eric A; Kazerooni, EA; MacMahon, H; van Beek, EJR; Yankelevitz, D; Biancardi, AM; Bland, PH; Brown, MS; Engelmann, RM; Laderach, GE, "Data from LIDC-IDRI," *The Cancer Imaging Archive (TCIA) Public Access*, 2015.

[17] M. A. Ribeiro, M. Varanis, A. M. Tusset, R. C. Machado, G. Litak, and J. M. Bathazar, "Performance analysis of a nonlinear energy harvester with subharmonic responses based on discrete Meyer wavelet filtering scheme," *Journal of the Brazilian Society of Mechanical Sciences and Engineering*, vol. 46, no. 7, p. 411, Jul. 2024, doi: 10.1007/s40430-024-04977-w.

[18] V. Gowthami, K. B. Bagan, and S. E. P. Pushpa, "A novel approach towards high-performance image compression using multilevel wavelet transformation for heterogeneous datasets," *The Journal of Supercomputing*, vol. 79, no. 3, pp. 2488–2518, Feb. 2023, doi: 10.1007/s11227-022-04744-5.

[19] D. K. Hammond, P. Vandergheynst, and R. Gribonval, "Wavelets on graphs via spectral graph theory," *Applied and Computational Harmonic Analysis*, vol. 30, no. 2, pp. 129–150, Mar. 2011, doi: 10.1016/j.acha.2010.04.005.

[20] Y.-J. Ma, Y. Ren, P. Feng, P. He, X.-D. Guo, and B. Wei, "Sinogram denoising via attention residual dense convolutional neural network for low-dose computed tomography," *Nuclear Science and Techniques*, vol. 32, no. 4, p. 41, Apr. 2021, doi: 10.1007/s41365-021-00874-2.

[21] Y. Liu, "A method of CT image denoising based on residual encoder-decoder network," *Journal of Healthcare Engineering*, vol. 2021, pp. 1–9, Sep. 2021, doi: 10.1155/2021/2384493.

[22] H. Shan *et al.*, "3-D convolutional encoder-decoder network for low-dose CT via transfer learning from a 2-D trained network," *IEEE Transactions on Medical Imaging*, vol. 37, no. 6, pp. 1522–1534, Jun. 2018, doi: 10.1109/TMI.2018.2832217.

[23] G. Wang and X. Hu, "Low-dose CT denoising using a progressive Wasserstein generative adversarial network," *Computers in Biology and Medicine*, vol. 135, p. 104625, Aug. 2021, doi: 10.1016/j.compbiomed.2021.104625.

[24] S. Bera and P. K. Biswas, "Noise conscious training of non local neural network powered by self attentive spectral normalized markovian Patch GAN for low dose CT denoising," *IEEE Transactions on Medical Imaging*, vol. 40, no. 12, pp. 3663–3673, Dec. 2021, doi: 10.1109/TMI.2021.3094525.

[25] Y. Zhang *et al.*, "(Double) Structure-preserving low-dose computed tomography image denoising using a deep residual adaptive global context attention network," *Quantitative Imaging in Medicine and Surgery*, vol. 13, no. 10, pp. 6528–6545, Oct. 2023, doi: 10.21037/qims-23-194.

[26] D. K. Hammond, P. Vandergheynst, and R. Gribonval, "The spectral graph wavelet transform: fundamental theory and fast computation," in *Vertex-Frequency Analysis of Graph Signals*, Springer, 2018, pp. 141–175. doi: 10.1007/978-3-030-03574-7_3.

BIOGRAPHIES OF AUTHORS

Iwan Setiawan received the M.Eng. degree in received the M.Eng. degree in instrumentation and control from Bandung Institute of Technology, Indonesia. Currently, he works as a researcher at the research center for artificial intelligence and cyber security, national research and innovation agency in Indonesia. His research interests include graph theory, wavelet, and their application in image processing. He can be contacted at email: iwan022@brin.go.id.

Rachmat Hidayat received the M.Sc. degree in computer science from University of Indonesia. Currently, he works as a researcher at the research center for artificial intelligence and cyber security, national research and innovation agency in Indonesia. He can be contacted at email: rach018@brin.go.id.

Abdul Mahatir Najar received the M.Sc. degree in applied mathematics from Sepuluh Nopember Institute of Technology, Indonesia. Currently, he works as a lecture at department of mathematics, University of Tadulako in Indonesia. He can be contacted at email: abdulmahatir@untad.ac.id.

Agus Indra Jaya received the M.Sc. degree in applied mathematics from University of Twente, the Netherlands. Currently, he works as a senior lecture at department of mathematics, University of Tadulako in Indonesia. He can be contacted at email: jayaindraagus@gmail.com.

Didi Rosiyadi hold a Ph.D. degree in information security from National Taiwan University of Science and Technology. Currently, he is a research professor at the research center for artificial intelligence and cyber security, national research and innovation agency in Indonesia. He can be contacted at email: didi016@brin.go.id.